J. Fluid Mech. (2001), *vol.* 432, *pp.* 351–367. Printed in the United Kingdom

Finite-amplitude convection in the presence of finitely conducting boundaries

By M. WESTERBURG AND F. H. BUSSE

Institute of Physics, University of Bayreuth, D-95440 Bayreuth, Germany

(Received 12 April 2000 and in revised form 4 October 2000)

Finite-amplitude convection in the form of rolls and their stability with respect to infinitesimal disturbances is investigated in the case of boundaries of the horizontal fluid layer which exhibit a thermal conductivity comparable to that of the fluid. It is found that even when rolls represent the preferred mode at the onset of convection a transition to square cells may occur at slightly supercritical Rayleigh numbers. The phenomenon of inertial convection in low Prandtl number fluids appears to become more pronounced as the conductivity of the boundaries is reduced. Modulated convection rolls have also been found as solutions of the problem. But they appear to be unstable in general. Experimental observations have been made and are found in general agreement with the theoretical predictions.

1. Introduction

Rayleigh–Bénard convection in a fluid layer heated from below has been analysed in much detail in the past few decades as a representative example of the formation of dynamical structures in fluids. But attention has usually been focused on the case of infinitely conducting boundaries, which can be described most simply from a theoretical point of view. While experimenters have strived to approach this ideal limit, a finite ratio λ between the thermal conductivity of the boundary and that of the fluid is always realized in experiments. In geophysical and engineering applications the conductivity of the boundary is often comparable to that of the fluid and so there exists considerable interest in the influence of finite values of λ.

The variation with λ of the critical value R_c of the Rayleigh number for the onset of convection is well known from Sparrow, Goldstein & Jonsson (1964), Jakeman (1968) and others. See also the discussion in the book of Gershuni & Zhukovitskii (1976). The preference for square cells instead of rolls was found by Busse & Riahi (1980) in the limit of vanishing λ and was later generalized to the case of finite λ and asymmetric boundary conditions by Riahi (1985).

Most of the work on nonlinear properties of convection in the presence of boundaries of finite conductivity has been restricted to the weakly nonlinear limit. In this paper we shall go beyond the neighbourhood of the critical Rayleigh number and analyse convection rolls and their instabilities for an extensive range in the Rayleigh, Prandtl and wavenumber parameter space. After the formulation of the basic equations and of the mathematical method for their solution in § 2, stationary two-dimensional solutions are discussed in § 3. An analysis of their stability follows in § 4 and in § 5 the phenomenon of inertial convection is studied. The results of an experiment are reported in § 6. A concluding discussion is given in the last section of the paper.

2. Mathematical formulation of the problem

We consider a horizontal fluid layer of height d heated from below. The average temperature at the upper and lower boundaries is T_1 and T_2, respectively. Using d as length scale, d^2/κ as time scale, where κ is the thermal diffusivity, and $T_2 - T_1$ as scale of the temperature we can write the equations of motion for the velocity vector $\boldsymbol{u}$ and the heat equations for the deviation Θ of the temperature from its distribution in the static case in dimensionless form:

$$\left(\frac{\partial}{\partial t}\boldsymbol{u} + \boldsymbol{u}\cdot\nabla\boldsymbol{u}\right) P^{-1} = -\nabla\pi + R\Theta\boldsymbol{k} + \nabla^2\boldsymbol{u}, \tag{1a}$$

$$\nabla\cdot\boldsymbol{u} = 0, \tag{1b}$$

$$\frac{\partial}{\partial t}\Theta + \boldsymbol{u}\cdot\nabla\Theta = \boldsymbol{u}\cdot\boldsymbol{k} + \nabla^2\Theta, \tag{1c}$$

where the Rayleigh number R and the Prandtl number P have their usual definitions:

$$R = \frac{\gamma g(T_2 - T_1)d^3}{\kappa\nu}, \quad P = \frac{\nu}{\kappa}.$$

Here, γ, g and ν denote the thermal expansivity, the acceleration due to gravity and the kinematic viscosity, respectively. The Boussinesq approximation has been used in that a constant density has been assumed except in the gravity term. We shall use a Cartesian system of coordinates with z-coordinate in the direction of the vertical unit vector $\boldsymbol{k}$. The conditions at the rigid top and bottom boundaries require

$$\boldsymbol{u} = 0, \quad \Theta = \hat{\Theta}, \quad \frac{\partial}{\partial z}\Theta = \lambda\frac{\partial}{\partial z}\hat{\Theta} \qquad \text{at } z = \pm\tfrac{1}{2}, \tag{2}$$

where $\hat{\Theta}$ is the deviation from the static temperature distribution at the boundaries. There exist a large variety of ways in which boundaries can be arranged such that the temperature distribution of the state of pure conduction depends only on z. We shall assume for simplicity the simplest configuration in which the boundaries are represented by half-spaces of uniform thermal conductivity which exceeds that of the fluid by the factor λ. The horizontal temperature variation will penetrate into the half-spaces only for a distance of the order d unless λ becomes very small such that large-wavelength convection becomes preferred. Accordingly the properties of the boundaries at a distance larger than d from the fluid layer will have little influence on the convection flow as long as they are uniform in the horizontal dimensions. We thus can assume that the computations presented in this paper will be representative for a variety of other boundary configurations. To eliminate the equation of continuity (1b) it is convenient to use the general representation for the solenoidal vector field $\boldsymbol{u}$,

$$\boldsymbol{u} = \nabla\times(\nabla\times\boldsymbol{k}\varphi) + \nabla\times\boldsymbol{k}\psi \equiv \boldsymbol{\delta}\varphi + \boldsymbol{\epsilon}\psi \tag{3}$$

and to take the z-components of the curl curl and the curl of equation (1a):

$$\left[\frac{\partial}{\partial t}\nabla^2\Delta_2\varphi + \boldsymbol{\delta}\cdot(\boldsymbol{u}\cdot\nabla\boldsymbol{u})\right] P^{-1} = -R\Delta_2\Theta + \nabla^4\Delta_2\varphi, \tag{4a}$$

$$\left[\frac{\partial}{\partial t}\Delta_2\psi + \boldsymbol{\epsilon}\cdot(\boldsymbol{u}\cdot\nabla\boldsymbol{u})\right] P^{-1} = \nabla^2\Delta_2\psi. \tag{4b}$$

Without losing generality we can impose the condition that the average of φ, ψ over the (x, y)-plane vanishes. Two-dimensional steady solutions of the system of equations

(1*c*) and (4) can be obtained in the form

$$\varphi(x,z) = \sum_{m,n=1}^{\infty} a_{mn} \cos(m\alpha x) f_n(z), \tag{5a}$$

$$\Theta(x,z) = \sum_{m=0,\,n=1}^{\infty} b_{mn} \cos(m\alpha x) h_{mn}(z), \tag{5b}$$

where $f_n(z)$ denotes the Chandrasekhar (1961) functions,

$$f_n(z) = \begin{cases} \dfrac{\cosh\beta_n z}{\cosh\beta_n/2} - \dfrac{\cos\beta_n z}{\cos\beta_n/2} & \text{for odd } n \\ \dfrac{\sinh\beta_n z}{\sinh\beta_n/2} - \dfrac{\sin\beta_n z}{\sin\beta_n/2} & \text{for even } n, \end{cases} \tag{6}$$

and the functions $h_{mn}(z)$ are defined by

$$h_{mn}(z) = \begin{cases} \sin n\pi z & \text{for } m = 0 \text{ and for even } n \\ \cos\gamma_{mn} z & \text{for } m \neq 0 \text{ and for odd } n \\ \sin\gamma_{mn} z & \text{for } m \neq 0 \text{ and for even } n, \end{cases} \tag{7}$$

Note that the summation in (5*b*) starts at $m = 0$ since Θ includes the change in the profile of the mean temperature. The quantities γ_{mn} are determined such that the boundary condition (2) for Θ is satisfied together with the solution

$$\hat{\Theta} = \sum_{m=1,\,n=1}^{\infty} b_{mn} h_{mn}(\pm\tfrac{1}{2}) \exp\{\mp m\alpha(z \mp \tfrac{1}{2})\} + \lambda(z \mp \tfrac{1}{2}) \times \sum_{n=\text{even}}^{\infty} b_{0n} n\pi(-1)^{n/2} \quad \text{for } z \begin{cases} > \tfrac{1}{2} \\ < -\tfrac{1}{2} \end{cases} \tag{8}$$

at the boundaries:

$$\gamma_{mn} \tan(\tfrac{1}{2}\gamma_{mn}) = \lambda m\alpha \quad \text{for odd } n \tag{9a}$$

$$\gamma_{mn} \cot(\tfrac{1}{2}\gamma_{mn}) = -\lambda m\alpha \quad \text{for even } n. \tag{9b}$$

There is no need to specify h_{0n} for odd n since for all solutions considered in this paper the mean temperature profile will be antisymmetric with respect to the midplane of the layer and thus all coefficients b_{0n} with odd n are vanishing. Moreover, we also use the symmetry property that the solutions bifurcating from the static state near the onset of convection exhibit vanishing coefficients whenever the sum $m + n$ of the subscripts m, n is odd. The quantities β_n obey the relationships

$$\tanh(\tfrac{1}{2}\beta_n) + \tan(\tfrac{1}{2}\beta_n) = 0 \quad \text{for odd } n \tag{10a}$$

$$\coth(\tfrac{1}{2}\beta_n) - \cot(\tfrac{1}{2}\beta_n) = 0 \quad \text{for even } n \tag{10b}$$

which ensure that the boundary conditions $\varphi = (\partial/\partial z)\varphi = 0$ at $z = \pm\frac{1}{2}$ are satisfied. For two-dimensional steady solutions $\psi \equiv 0$ holds as required by equation (4*b*) together with the boundary condition $\psi = 0$ at $z = \pm\frac{1}{2}$.

After representations (5) have been introduced into equations (1*c*) and (4*a*), we obtain nonlinear algebraic equations for the unknowns a_{mn}, b_{mn} by multiplying equations (1*c*) and (4*a*) by the expansion functions used in expressions (5*a*) and (5*b*), respectively, and averaging the result over the fluid layer. The system of nonlinear algebraic

equations can be solved by a Newton–Raphson iteration method after the infinite system has been truncated. We shall neglect all coefficients a_{mn}, b_{mn} and corresponding equations that satisfy

$$m + n > N_T, \tag{11}$$

where the truncation parameter N_T is chosen such that the solution does not change significantly when N_T is replaced by $N_T + 2$. Usually we shall require that the convective heat transport changes by less than 1% with this change of the truncation parameter. For the normal roll solutions values up to $N_T = 16$ proved to be sufficient. But in some low Prandtl number cases and for the modulated roll solutions discussed in the next section values up to $N_T = 22$ were used.

The stability of steady solutions of the form (5) can be analysed through the superposition of infinitesimal disturbances

$$\tilde{\varphi} = \sum_{m,n} \tilde{a}_{mn} \exp\{\mathrm{i}m\alpha x + \mathrm{i}by + \mathrm{i}dx + \sigma t\} f_n(z), \tag{12a}$$

$$\tilde{\psi} = \sum_{m,n} \tilde{c}_{mn} \exp\{\mathrm{i}m\alpha x + \mathrm{i}by + \mathrm{i}dx + \sigma t\} \sin n\pi(z + \tfrac{1}{2}), \tag{12b}$$

$$\tilde{\Theta} = \sum_{m,n} \tilde{b}_{mn} \exp\{\mathrm{i}m\alpha x + \mathrm{i}by + \mathrm{i}dx + \sigma t\} \tilde{h}_{mn}(z), \tag{12c}$$

where the functions $\tilde{h}_{mn}(z)$ are given by

$$\tilde{h}_{mn}(z) = \begin{cases} \cos \tilde{\gamma}_{mn} z & \text{for odd } n \\ \sin \tilde{\gamma}_{mn} z & \text{for even } n \end{cases} \tag{13}$$

and where the $\tilde{\gamma}_{mn}$ are defined as the roots of the equations

$$\tilde{\gamma}_{mn} \tan(\tfrac{1}{2}\tilde{\gamma}_{mn}) = ((m\alpha + d)^2 + b^2)^{\frac{1}{2}} \lambda \quad \text{for odd } n, \tag{14a}$$

$$\tilde{\gamma}_{mn} \cot(\tfrac{1}{2}\tilde{\gamma}_{mn}) = -((m\alpha + d)^2 + b^2)^{\frac{1}{2}} \lambda \quad \text{for even } n. \tag{14b}$$

The representation (12c) together with the definitions (13), (14) guarantees that the disturbance $\tilde{\Theta}$ is matched correctly to the corresponding steady solution at the boundaries. The representation (12c) thus becomes correct only in the special case $\sigma = 0$. Since most instabilities of interest are characterized by a vanishing imaginary part σ_i of σ and since we are interested in the stability boundary at which the real part σ_r of σ changes sign the restriction to $\sigma = 0$ is not a serious one. For $\sigma \neq 0$ the representation (12) will still give approximately correct results as long as $|\sigma|$ is not large compared to $(\alpha + d)^2 + b^2$.

3. Steady convection in the form of rolls

Rolls described by two-dimensional solutions of the form (5) represent the simplest form of convection and are often realized in experiments when the critical value of the Rayleigh number is exceeded and when the asymmetry with respect to the midplane of the layer vanishes. In the present case of finitely conducting boundaries the structure of the isotherms becomes a striking feature of the solution. As the convection flow distorts the originally horizontally oriented isotherms it pulls in additional isotherms from the weakly conducting boundaries such that the orientation of the isotherms

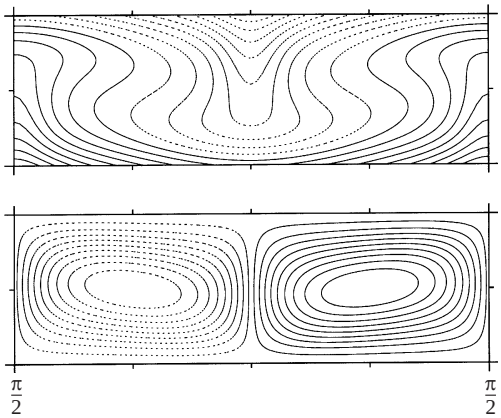

FIGURE 1. Isotherms (top) and streamlines (bottom) of convection rolls in the case $P = 0.71$, $\lambda = 0.1$, $R = 5000$, $\alpha = 2.0$. Solid (dashed) curves indicate positive (negative) values.

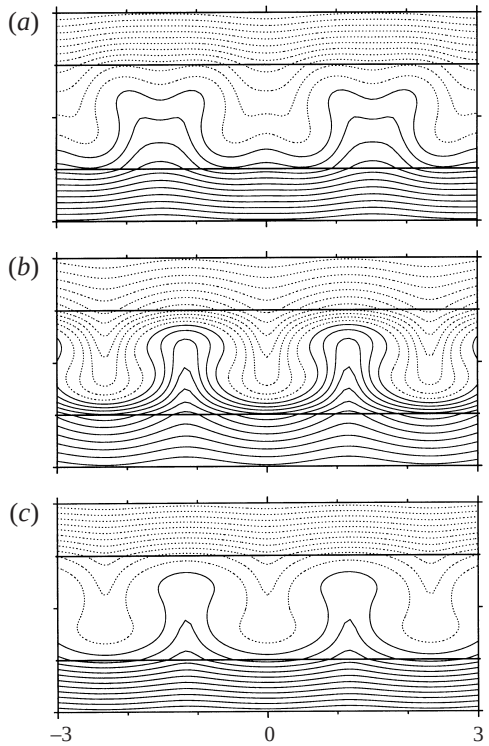

FIGURE 2. Isotherms of convection rolls between boundaries for which the thermal conductivity differs by the ratio λ from that of the fluid. (*a*) $P = 0.01$ with $\lambda = 0.5$ and $\alpha = 2.071$; (*b*) $P = 0.71$ with $\lambda = 2$ and $\alpha = 2.705$; and (*c*) $P = 0.71$ with $\lambda = 0.5$, $\alpha = 2.705$. The boundary region adjacent to the layer is also shown. $R = 5000$ in all cases.

becomes predominantly vertical as can be seen in figure 1. Since the deviations from the horizontal isotherms of the basic static state occur over a larger height than that of the fluid layer, the wavelength of the convection rolls becomes larger with decreasing λ and the critical value R_c of the Rayleigh number is also reduced. From

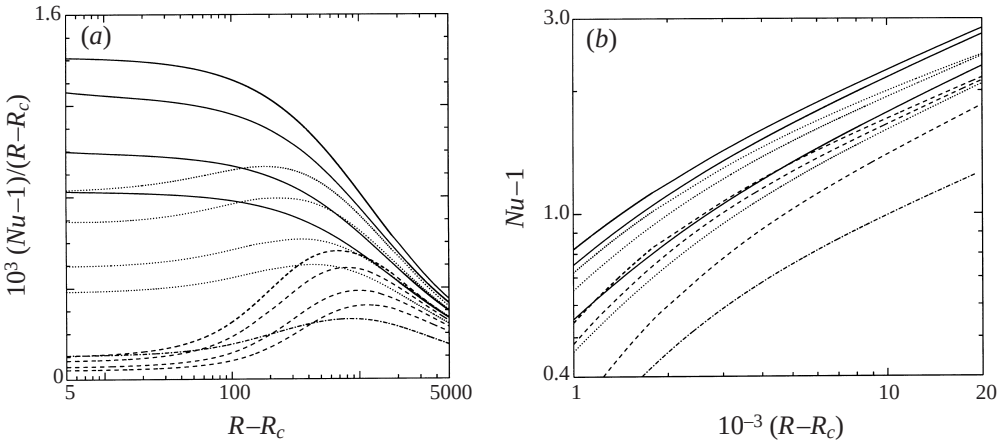

FIGURE 3. (*a*) The Nusselt number Nu as a function of the Rayleigh number R for the Prandtl numbers $P = 0.71$ (solid lines), $P = 0.1$ (dotted lines) and $P = 0.025$ (dashed lines). The four lines in each case correspond to $\lambda = 0.4, 1, 4, \infty$ (from top to bottom on the left-hand side) always with $\alpha = 3.0$. The dash-dotted line corresponds to the critical value $\alpha_c = 1.96$ in the case $P = 0.025, \lambda = 0.4$. (*b*) As (*a*) but for large R. The sequence of lines for each of the three Prandtl number cases is given by $\lambda = 0.4, 1, \infty$ (from top to bottom).

the mathematical point of view the decrease of the eigenvalue R_c of the linear problem is caused, of course, by the weakening of the boundary condition (2) for Θ as λ is decreased from infinity to zero. Some other examples of isotherms of convection rolls are shown in figure 2 where parts of the solid boundaries are shown as well in order to provide a more realistic picture of the temperature distribution. It is of interest to see that the hot and cold plumes tend to exhibit a double structure as the Prandtl number is decreased.

While the structure of the isotherms differs considerably for boundaries of low and of high thermal conductivity, the convective heat transport varies more with the Prandtl number than with the parameter λ, as is evident from figure 3(*a*). In figures 3(*a*) and 3(*b*) all lines except for one correspond to the same wavenumber in order to facilitate the comparison. If the critical value of the wavenumber α is used the heat transport in the cases of boundaries with low conductivity no longer exceeds the transport in the case of highly conducting boundaries except close to the onset of convection. Thus the sequence of the heat transports as a function of λ becomes reversed, at least in the cases $P = 0.1$ and $P = 0.025$, when the critical value of α is used instead of a fixed value. The fact that low-conducting boundaries do not inhibit the heat transport in the fluid layer more significantly must be attributed to the property that the convective transport given by the horizontal average $\overline{u_z\Theta}$ penetrates closer to the boundaries since only u_z must vanish there, while both u_z and Θ vanish at the infinitely conducting boundary.

A special feature of convection in the presence of finitely conducting boundaries is that many types of modulated roll solutions exist besides the normal periodic arrangement of convection rolls. Examples of various coexisting rolls of different size at the same external conditions are shown in figure 4(*a*, *b*). Obviously, the soft boundary conditions for the temperature field promote an arrangement where weak small rolls coexist in a steady equilibrium with strong larger rolls. The solution branches of modulated rolls are connected through bifurcations with solution branches of strictly periodic rolls as shown, for example, in figure 5. Here an additional branch

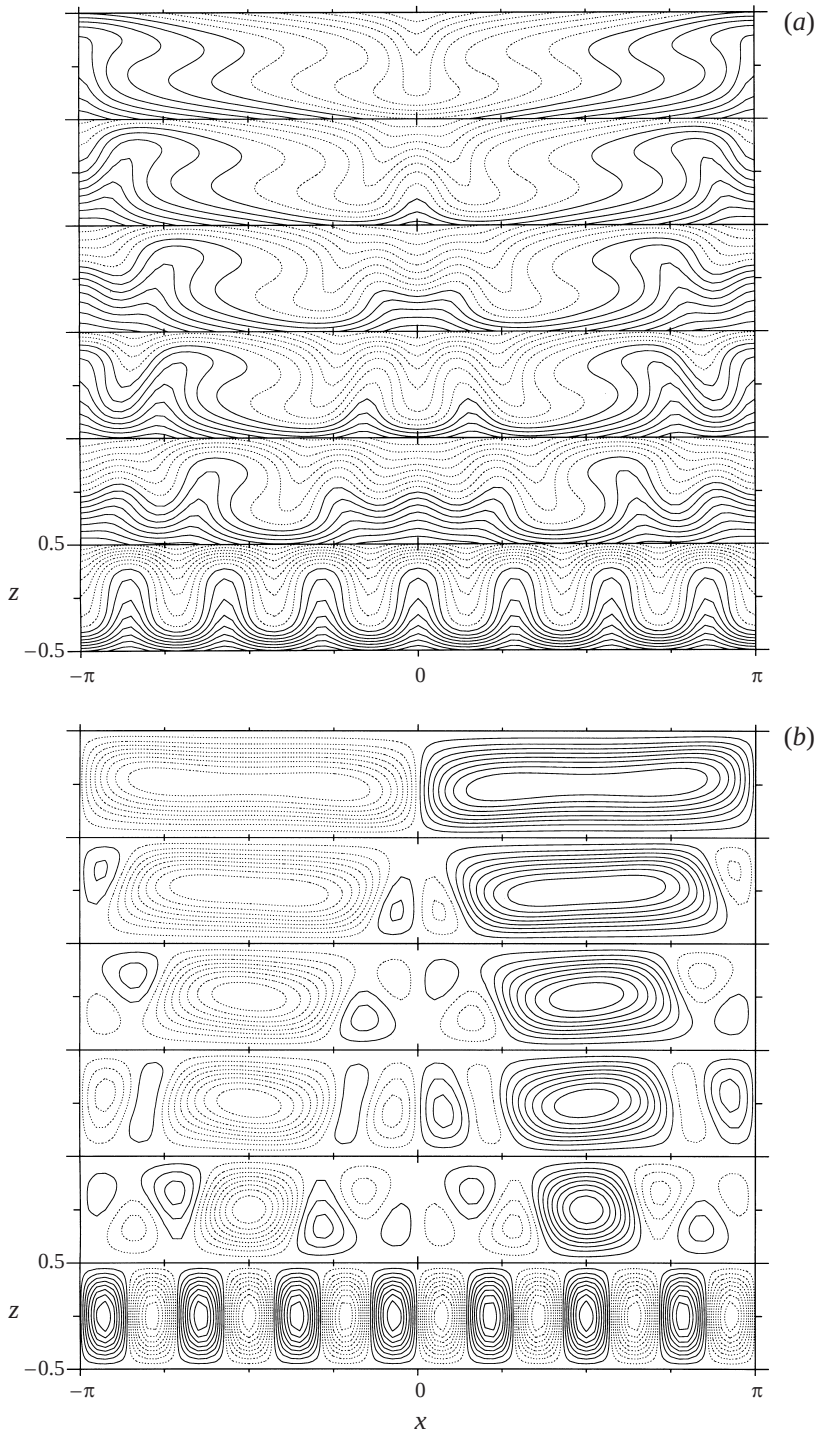

FIGURE 4. (*a*) Isotherms and (*b*) streamlines of simply periodic (uppermost and lowermost panel) and of modulated periodic convection rolls in the case $R = 10000$, $\alpha = 1$, $P = 0.71$ and $\lambda = 1$.

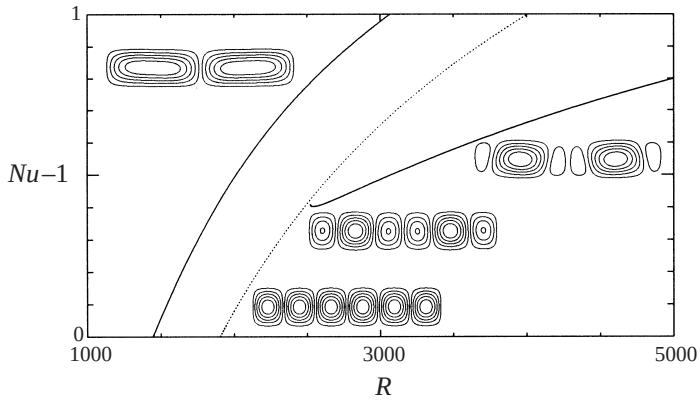

FIGURE 5. The Nusselt number Nu as a function of the Rayleigh number in the case $P = 0.71$, $\lambda = 1$. The left solid line and the dotted line correspond to rolls with the wavenumbers $\alpha = 1.5$ and $\alpha = 4.5$, respectively. Modulated rolls bifurcate from the rolls with $\alpha = 4.5$ as indicated in the figure. The flow is downward in the middle of each streamline pattern.

of periodic rolls with $\alpha = 7.5$ (instead of $\alpha = 4.5$) could have been computed from which a branch of modulated rolls would bifurcate with one dominant roll pair and four weaker roll pairs (instead of two weaker roll pairs as shown in the figure). But because all modulated roll solutions were found to be unstable, only selected cases have been computed. Modulated rolls have also been found in an analysis of convection with fixed temperatures at the boundaries (Mizushima & Fujimura 1992).

4. Instabilities of steady roll solutions

Because of the large number of parameters involved in the problem, the stability of steady two-dimensional convection solutions has been analysed only with respect to disturbances of the form (12) with $d = 0$. Since it is known from earlier studies (see, for example, Bolton, Busse & Clever 1986) of the stability of convection rolls in the presence of infinitely conducting boundaries that disturbances with $d = 0$ are the most important ones in most of the parameter space of the problem, the assumption $d = 0$ does not seem to be too restrictive. The Eckhaus instability has been disregarded in this way, but it usually does not limit the region of stable rolls in the parameter space. The neglect of the skewed varicose instability is more serious and must be kept in mind when the theoretical results are compared to future experimental observations.

The main goal of the stability analysis has been the understanding of the transition from rolls to square convection at supercritical Rayleigh numbers. This transition is accomplished by the cross-roll instability which corresponds to $d = 0$. Rolls at a right angle to the given rolls grow in this case until convection in the form of a square pattern or a rectangular pattern is realized. We start by considering the case of $P = 450$ shown in figure 6. This Prandtl number is representative of large P values and the results hardly differ from the case $P = \infty$. Beginning with the classical case of infinitely conducting boundaries, $\lambda = \infty$, this figure demonstrates how the region of stable steady roll convection shrinks as λ is decreased. It is remarkable how similar the stability regions are for different values of λ. This property is peculiar to the limit of high Prandtl number and reflects the property that only the nonlinear term of the heat equation enters the analysis at high values of P. The zig-zag instability which limits the region of stable rolls to smaller values of α depends very little on

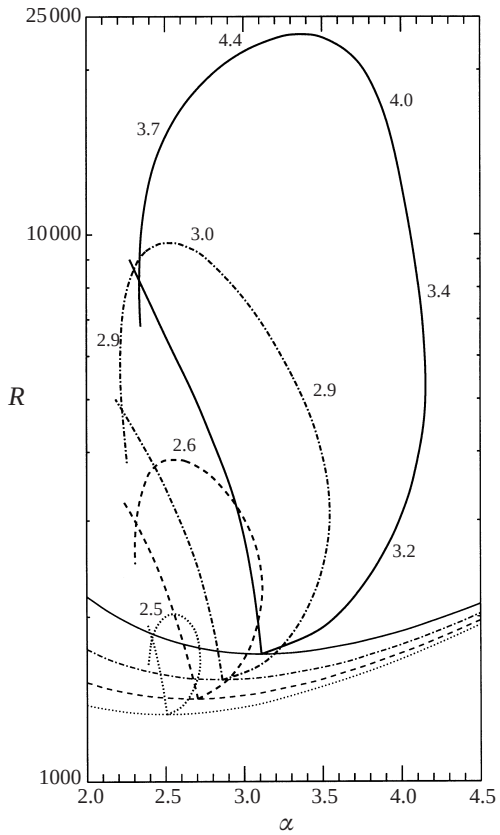

FIGURE 6. Stability boundaries in the (R, α)-plane for two-dimensional rolls in the case $P = 450$ for $\lambda = \infty$ (solid lines), $\lambda = 4$ (dashed-dotted lines), $\lambda = 2$ (dashed lines), $\lambda = 1.3$ (dotted lines). The lowermost line indicates the neutral curve for the onset of convection for each λ. The stability regions are bounded by the onset of the cross-roll instability on the right-hand side with the numbers denoting the wavenumbers b of the growing disturbances, while the line on the left-hand side indicates the onset of the zig-zag instability in the limit of vanishing wavenumbers b.

λ, while the growth rate of the cross-roll instability increases with $|\alpha - \alpha_c|$ as well as with $R - R_c$ as λ is decreased. The region of stability thus contracts in a nearly self-similar way until square convection corresponding to the superposition of rolls and cross-rolls replaces rolls as stable form of convection at $R = R_c$. In figure 7 the stability boundaries are shown for the case $P = 7$ which exhibits a lesser degree of similarity. Again the region of stable rolls is much reduced as λ decreases towards the value where rolls are unstable even at the critical value R_c of the Rayleigh number according to the analysis of Riahi (1985).

In the $P = 0.71$ case shown in figure 8 the shape of the stability region changes considerably as λ is decreased from infinity. It is noteworthy that the stability region now extends as a narrow strip towards small wavenumbers. Because of numerical difficulties it was not possible to continue the computations to much lower wavenumber than those shown in the figure. Another feature of interest is that the onset of the oscillatory instability hardly depends on the conductivity ratio λ. This property is less surprising if it is remembered that the oscillatory instability is hydrodynamic (Busse 1972) and is only slightly influenced by thermal effects. Because this instability

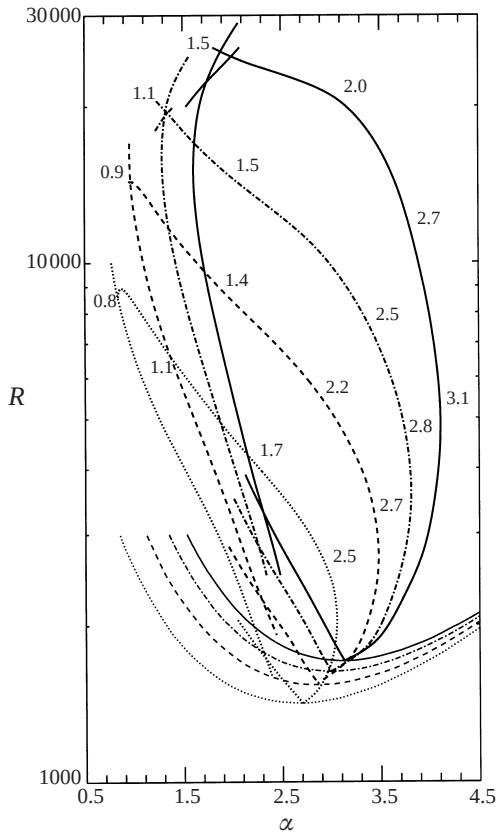

FIGURE 7. Same as figure 6, but in the case $P = 7$ for $\lambda = \infty$ (solid lines), $\lambda = 10$ (dash-dotted lines), $\lambda = 4$ (dashed lines), $\lambda = 2$ (dotted lines). The stability boundary on the right-hand side is now given by the knot instability characterized by values of $b < \alpha_c$, while the zig-zag instability provides the stability boundary of the left-hand side only for a small neighbourhood above $R = R_c$. The main part of the stability boundary on the left-hand side is described by the onset of cross-roll disturbances with wavenumbers b decreasing first from 2.5 to a minimum of 2.0 around $R = 4500$ and then increasing to 3.6 at $R = 10^4$.

requires a sufficiently high amplitude of motion, it does not occur for Rayleigh numbers less than about 5000 and thus is preceded by the knot instability for values of λ less than about 2. This latter instability exhibits the same symmetry properties as the cross-roll instability but is characterized by a smaller value of the disturbance wavenumber b (Busse & Clever 1979).

For Prandtl numbers of the order unity or less the skewed varicose instability usually limits the region of stable rolls to high wavenumbers. Since this instability has not been taken into account in the present analysis, the right-hand side of the region of stable rolls is more restricted than it may appear from the figures. In figure 8 this effect is probably not very important since the onset of the knot instability is shifted strongly towards the left with decreasing λ. But in the case of figure 9 for $P = 0.025$ the onset of the skewed varicose instability is likely to prevent stable rolls with wavenumbers α exceeding the value α_c by any significant amount. The stability of rolls becomes limited by a new branch of the cross-roll instability which sharply veers back from the left-hand branch and reduces the range of stable rolls with $\alpha = \alpha_c$ to zero as λ approaches values of the order 10^{-2}.

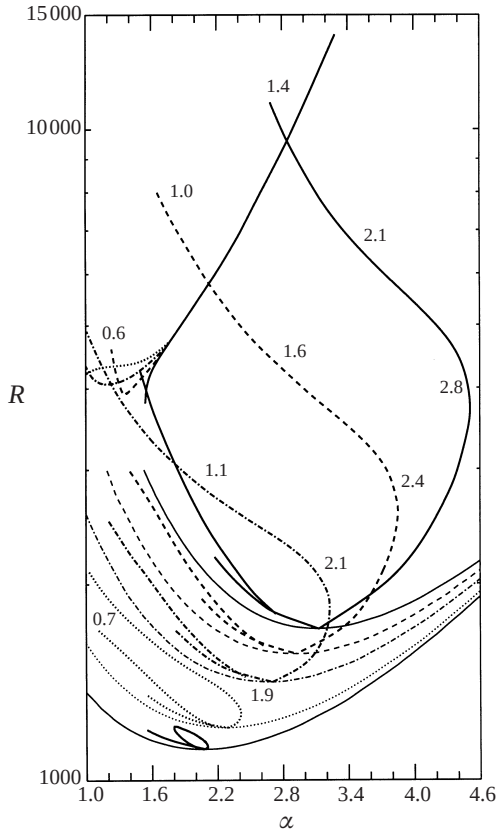

FIGURE 8. Same as figure 6, but in the case $P = 0.71$ for $\lambda = \infty$ (upper solid lines), $\lambda = 5$ (dashed lines), $\lambda = 2$ (dash-dotted lines), $\lambda = 0.75$ (dotted lines), $\lambda = 0.5$ (lower solid lines). The stability boundary on the right-hand side is given by the knot instability with b-wavenumbers indicated. The stability boundary on the left-hand side is given by the zig-zag instability in the neighbourhood of $R = R_c$ and by the cross-roll instability at higher values of R. The b-wavenumbers of this instability vary from $b \approx a_c$ at $R = R_c$ to about the same value at the upper end of the curve with a drop of 10% at the middle of the curve. Towards higher values of R the stability region is bounded by the onset of the oscillatory instability which depends on the parameter λ only at the low wavenumber end.

5. Inertial convection

Inertial or 'flywheel' convection is a typical phenomenon of low Prandtl number fluids that has received much attention from theoreticians, but has not yet been observed in experiments. Jones, Moore & Weiss (1976) first noticed that the convective heat transport which for low Prandtl number fluids varies in proportion to $P^2(R-R_c)$ (unless two-dimensional rolls with unrealistic stress-free boundaries are considered) exhibits a much stronger growth once a second critical Rayleigh number is exceeded. Associated with this transition is a transformation of the convection rolls from a sinusoidal dependence on the horizontal coordinate to a form in which the motion depends only on the distance from the axis of the roll. Analytical treatments of this phenomenon have been given by Proctor (1977) and by Busse & Clever (1981) and for a numerical analysis of two-dimensional convection in low Prandtl number fluids we refer to Clever & Busse (1981). The results obtained in the latter paper correspond to the limit $\lambda = \infty$ of the roll solutions described by expressions (5). In figure 10

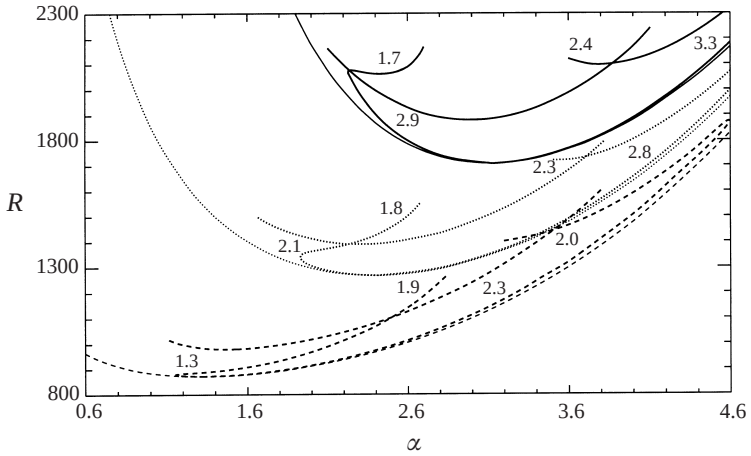

FIGURE 9. Same as figure 6, but in the case $P = 0.025$ for $\lambda = \infty$ (solid lines), $\lambda = 1$ (dotted lines), $\lambda = 0.1$ (dashed lines). The cross-roll instability has been characterized by the values of the b-wavenumber. The other stability boundary corresponds to the onset of the oscillatory instability.

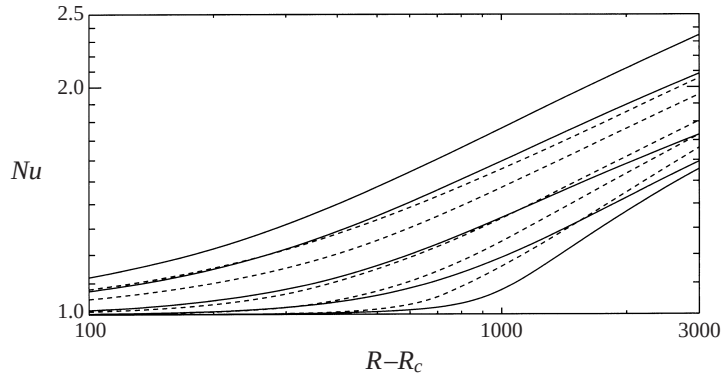

FIGURE 10. The Nusselt number Nu for two-dimensional convection with the critical wavenumber as function of R for $\lambda = 1$ (solid lines) and $\lambda = \infty$ (dashed lines, after Clever & Busse 1981). The lines correspond from top to bottom to $P = 0.71, 0.1, 0.025, 0.01$ and 0.003.

the heat transports by convection rolls obtained for low Prandtl numbers in the case $\lambda = 1$ have been compared with those for $\lambda = \infty$. It appears that the phenomenon of inertial convection persists in the case of finitely conducting boundaries and it even seems to be slightly enhanced.

The evolution towards the 'flywheel' form of convection rolls is demonstrated in figure 11 where the property is clearly seen that the flywheel rolls become separated by stagnant fluid if the wavenumber α is small enough. In the limit when the streamlines become exactly circular the left-hand side of equation (4a) vanishes and its inhibiting influence on the amplitude of motion disappears. Of course, because of the rigid boundaries, deviations from circular streamlines occur in the viscous boundary layers at top and bottom and ideal flywheel convection cannot be approached as closely as in the case of convection in a horizontal cylinder treated by Proctor (1977).

Unfortunately, the interesting phenomenon of inertial convection rolls cannot be easily realized in experiments because rolls are unstable with respect to three-dimensional disturbances at Rayleigh numbers much below those required for the

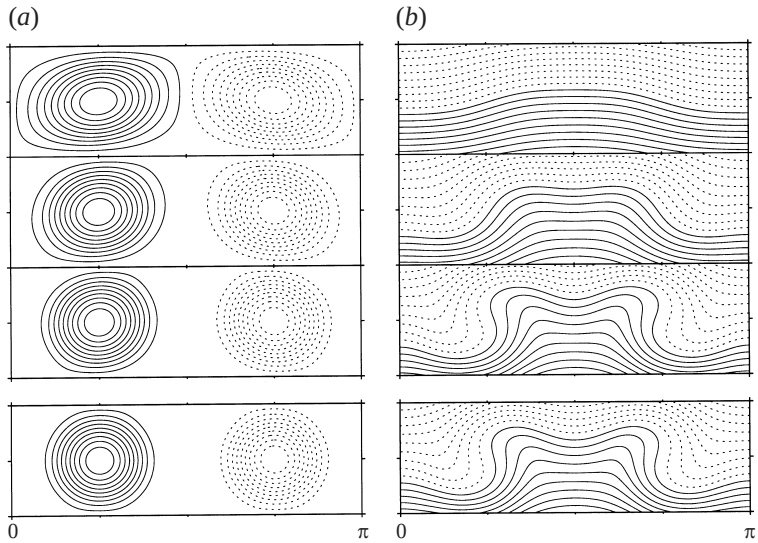

FIGURE 11. (*a*) Streamlines and (*b*) isotherms of convection rolls with $\alpha = 2.0$ in the case $\lambda = 0.5$, $P = 0.025$ for $R = 1300, 2000, 5000$ (top three plots) and in the case $\lambda = 0.5$, $P = 0.003$, $R = 5000$ (bottom plot).

Properties	Water/Plexiglas	Silicone oil/Plexiglas	Water/glass
Fluid layer thickness	5 mm	4 mm	5 mm
Temperature	22 °C	27 °C	21 °C
Boundary thickness	10 mm	10 mm	3 mm
Thermal conductivity of fluid	$0.605\,\mathrm{W\,mK^{-1}}$	$0.131\,\mathrm{W\,mK^{-1}}$	$0.605\,\mathrm{W\,mK^{-1}}$
Thermal expansivity γ	$2.27 \times 10^{-4}\,\mathrm{K^{-1}}$	$10.8 \times 10^{-4}\,\mathrm{K^{-1}}$	$2.17 \times 10^{-4}\,\mathrm{K^{-1}}$
Thermal diffusivity κ	$0.145\,\mathrm{mm^2\,s^{-1}}$	$0.0873\,\mathrm{mm^2\,s^{-1}}$	$0.145\,\mathrm{mm^2\,s^{-1}}$
Kinem. viscosity ν	$0.957\,\mathrm{mm^2\,s^{-1}}$	$5.02\,\mathrm{mm^2\,s^{-1}}$	$0.98\,\mathrm{mm^2\,s^{-1}}$
Boundary conductivity	$0.154\,\mathrm{W\,mK^{-1}}$	$0.154\,\mathrm{W\,mK^{-1}}$	$0.79\,\mathrm{W\,mK^{-1}}$
Eff. conductivity ratio λ^*	0.255	1.18	1.49

TABLE 1. Parameters of experiments.

transition to flywheel convection. There appears to be the possibility, however, of suppressing three-dimensional disturbances by employing the stabilizing effect of the Coriolis force. We shall comment on this possibility in the concluding section.

6. Experimental observations

In order to get an approximate comparison with the theoretical predictions some experiments have been carried out. An experimental apparatus and a shadowgraph visualization method similar to those used in the experiment of Busse & Whitehead (1971) have been used. A sketch of the experimental setup is shown in figure 12. The horizontal extent of the convection layer is only $430 \times 210\,\mathrm{mm^2}$ and thus much smaller than in the earlier experiment. Water and silicone oil have been used as convecting fluids the properties of which are listed in table 1. The fluid layer is bounded by 3 mm thick glass plates which separate it from the upper and lower channels through which thermostatically controlled water is pumped. In order to decrease the thermal

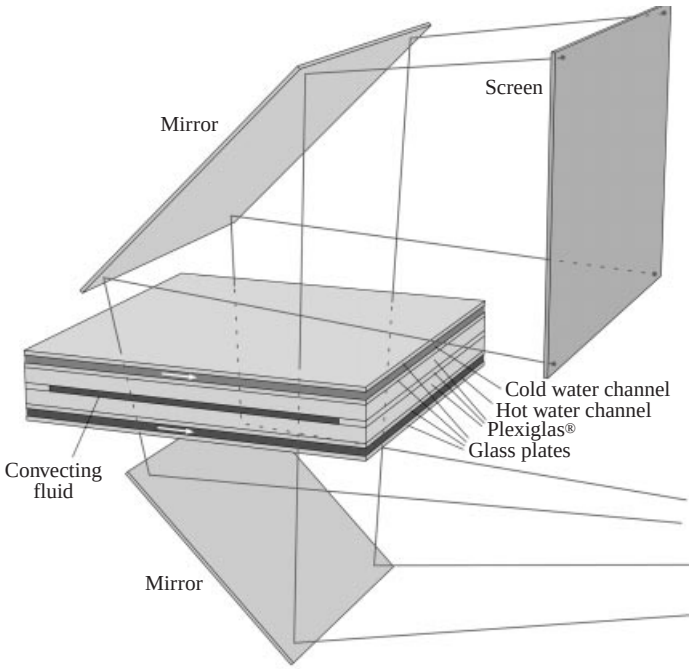

FIGURE 12. Sketch of the experimental apparatus.

conductance of the boundaries additional Plexiglas plates of 10 mm thickness can be inserted symmetrically above and below the convecting fluid. The experimental apparatus is thus similar to one that used in the experiment of Le Gal & Croquette (1988). Their layer was circular and had a smaller aspect ratio, but shadowgraph visualization was also used.

Since the vertical extent of the Plexiglas plates is finite while an infinite half-space has been assumed in the theory, the solution (8) must be modified. Assuming that the temperatures at the positions $z = \pm(\frac{1}{2} + \delta)$ are fixed we obtain instead of (8)

$$\hat{\Theta} = \sum_{m=1,n=1}^{\infty} b_{mn} h_{mn}(\pm\tfrac{1}{2}) \frac{\sinh m\alpha(z \mp (\frac{1}{2} + \delta)}{\sinh m\alpha(\mp\delta)} + \lambda(z \mp \tfrac{1}{2}) \times \sum_{n=\text{even}}^{\infty} b_{0n} n\pi(-1)^{n/2} \quad \text{for} \begin{cases} \frac{1}{2} + \delta > z > \frac{1}{2} \\ -\frac{1}{2} - \delta < z < -\frac{1}{2} \end{cases} \tag{15}$$

such that the boundary conditions (2) for Θ are satisfied with

$$\gamma_{mn} \tan(\tfrac{1}{2}\gamma_{mn}) = \lambda m\alpha \coth(m\alpha\delta) \quad \text{for odd } n \tag{16a}$$

$$\gamma_{mn} \cot(\tfrac{1}{2}\gamma_{mn}) = -\lambda m\alpha \coth(m\alpha\delta) \quad \text{for even } n \tag{16b}$$

instead of equations (9). For the linear theory of the onset of convection all terms with $m > 1$ can be neglected and equations (16) become identical to equations (9) in this case if λ is replaced by

$$\lambda^* \equiv \lambda \coth \alpha\delta. \tag{17}$$

It is difficult to measure the heat transport and the Rayleigh number in convection experiments with boundaries of low conductivity since the temperature difference

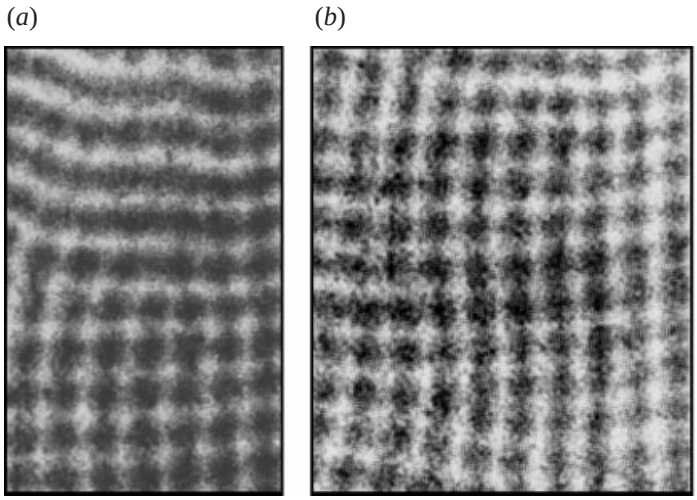

FIGURE 13. Shadowgraph images of (*a*) coexisting rolls and squares and (*b*) square pattern convection observed in a layer of silicone oil bounded by Plexiglas plates. The Rayleigh number exceeds the critical value by about 20% in (*a*) and by about 50% in (*b*). In both cases the patterns are essentially stationary for several hours.

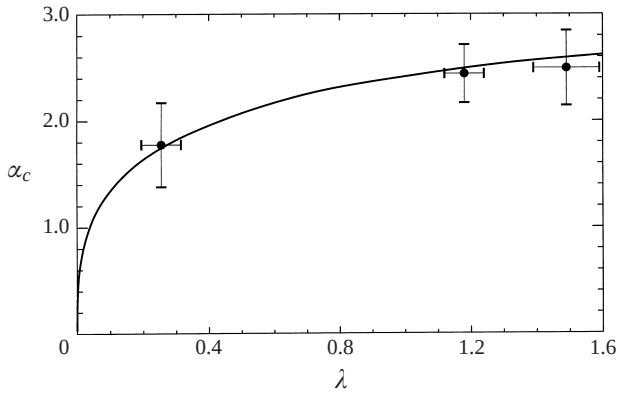

FIGURE 14. The wavenumber α as a function of the conductivity ratio λ between boundary and fluid. The solid line indicates the result of the linear theory for the onset of convection. The measurement points correspond the cases of water with Plexiglas boundaries, silicone oil with Plexiglas boundaries, and water with glass boundaries (from left to right). For the experimental values the rescaled value λ^* given by (17) has been used.

across the fluid layer is only a small fraction of the measured difference between the thermostatically controlled outer boundaries. Hence the experimental observations have focused on those properties of convection which do not depend strongly on R. In the case of water with Plexiglas boundaries convection in the form of square cells is observed, while rolls are seen in the case of plate glass boundaries, which agrees with the predictions of the weakly nonlinear theory (Riahi 1985). The case of silicone oil with Plexiglas boundaries is of special interest since an onset of convection in the form of rolls and a transition to square cells at a slightly supercritical Rayleigh number is predicted. The experimental observations do indeed indicate an onset of rolls and a regime of coexistence of rolls and square cells at supercritical Rayleigh numbers as shown by figure 13(*a*). This phenomenon could be an indication of a

hysteretic transition from rolls to squares with increasing R. At much higher values of R of the order of a few times the critical value a second transition with a return from square convection to roll-like convection appears to occur. Such a transition has not been observed in the case of water with Plexiglas boundaries. The wavelength of roll as well as square pattern convection has been measured and is found in reasonable agreement with the prediction of the linear theory for the onset of convection as shown in figure 14. The wavenumber in the case of water with Plexiglas boundaries is lower than the value 2.5 measured by Le Gal & Croquette (1988) under rather similar conditions. But because of the small aspect ratio the size of their square convection cells varies considerably and strongly decreases towards the sidewalls.

7. Concluding remarks

The influence of the finite thermal conductivity of the upper and lower boundaries is usually neglected in theoretical treatments of Rayleigh–Bénard convection in order to avoid the introduction into the problem of an additional parameter. As can be seen from the present study and other recent ones focusing on the influence of asymmetric boundaries (Clever & Busse 1995, 1998) the reducing of the ratio λ between the conductivities of the fluid and boundaries has profound effects on the dynamics of convection and on its horizontal planform in particular. On decreasing λ the temperature field decouples to some extent from the velocity field and thus more general solutions than just simply periodic rolls become possible. Although solutions of this kind as displayed in figures 4(a) and 4(b) have been found to be unstable in the two-dimensional case, an even richer variety of solutions must be expected in the three-dimensional case. Eventually these modulated solutions could be stabilized in layers of finite aspect ratio.

One of the motivations of the present paper has been the question of the realizibility of the phenomenon of inertial convection in an experiment. Because of the required low Prandtl number only convection in liquid metals offers the chance of a successful experiment. In this case high values of λ cannot be attained and the question arises whether inertial convection persists when the conductivity ratio λ is reduced to values of the order unity. The analysis of § 5 has given an affirmative answer to this question. The second obstacle to an experimental realization are the three-dimensional instabilities of convection rolls in a low Prandtl number fluid. By using the configuration of a rotating cylindrical annulus we hope to overcome this obstacle eventually. As demonstrated in an earlier experiment (Busse & Carrigan 1974) convection driven by centrifugal buoyancy in the annular gap between a cooled inner and a heated outer cylinder assumes the form of two-dimensional rolls parallel to the axis of rotation. Since the Coriolis force exerts a dominating influence on convection in a rapidly rotating cylindrical annulus it is expected that the transition to inertial convection can indeed be observed in such an experiment.

REFERENCES

Bolton, E. W., Busse, F. H. & Clever, R. M. 1986 Oscillatory instabilities of convection rolls at intermediate Prandtl numbers. *J. Fluid Mech.* **164**, 469–485.

Busse, F. H. 1972 The oscillatory instability of convection rolls in a low Prandtl number fluid. *J. Fluid Mech.* **52**, 97–112.

Busse, F. H. & Carrigan, C. R. 1974 Convection induced by centrifugal buoyancy. *J. Fluid Mech.* **62**, 579–592.

Busse, F. H. & Clever, R. M. 1979 Instabilities of convection rolls in a fluid of moderate Prandtl number. *J. Fluid Mech.* **91**, 319–335.

Busse, F. H. & Clever, R. M. 1981 An asymptotic model of two-dimensional convection in the limit of low Prandtl number. *J. Fluid Mech.* **102**, 75–83.

Busse, F. H. & Riahi, N. 1980 Nonlinear convection in a layer with nearly insulating boundaries. *J. Fluid Mech.* **96**, 243–256.

Busse, F. H. & Whitehead, J. A. 1971 Instabilities of convection rolls in a high Prandtl number fluid. *J. Fluid Mech.* **47**, 305–320.

Chandrasekhar, S. 1961 *Hydrodynamic and Hydromagnetic Stability*. Oxford: Clarendon.

Clever, R. M. & Busse, F. H. 1981 Low Prandtl number convection in a layer heated from below. *J. Fluid Mech.* **102**, 61–74.

Clever, R. M. & Busse, F. H. 1995 Convection rolls and their instabilities in the presence of a nearly insulating upper boundary. *Phys. Fluids* **7**, 92–97.

Clever, R. M. & Busse, F. H. 1998 Convection in a layer heated from below with a nearly insulating boundary. *Phys. Rev.* E **57**, 4198–4205.

Gershuni, G. Z. & Zhukovitskii, E. M. 1976 *Convective Stability of Incompressible Fluids* (translated from Russian by D. Louvish). Keter, Jerusalem.

Jakeman, E. 1968 Convective instability in fluids of high thermal diffusivity. *Phys. Fluids* **11**, 10–14.

Jones, C. A., Moore, D. R. & Weiss, N. O. 1976 Axisymmetric convection in a cylinder. *J. Fluid Mech.* **73**, 353–388.

Le Gal, P. & Croquette, V. 1988 Appearance of a square pattern in a Rayleigh–Bénard experiment. *Phys. Fluids* **31**, 3440–3442.

Mizushima, J. & Fujimura, K. 1992 Higher harmonic resonance of two-dimensional disturbances in Rayleigh–Bénard convection. *J. Fluid Mech.* **234**, 651–667.

Proctor, M. R. E. 1977 Inertial convection at low Prandtl number. *J. Fluid Mech.* **82**, 97–114.

Riahi, N. 1985 Nonlinear thermal convection with finite conducting boundaries. *J. Fluid Mech.* **152**, 113–123.

Sparrow, E. M., Goldstein, R. J. & Jonsson, V. K. 1964 Thermal instability in a horizontal fluid layer: effect of boundary conditions and nonlinear temperature profile. *J. Fluid Mech.* **18**, 513–528.